The response of carbon nanotube ensembles to fluid flow: Applications to mechanical property measurement and diagnostics

C. P. Deck,[1] C. Ni,[1] K. S. Vecchio,[1,2] and P. R. Bandaru[1,3,a)]
[1]*Materials Science and Engineering Program, University of California, San Diego, California 92093, USA*
[2]*Department of NanoEngineering, University of California, San Diego, California 92093-0448, USA*
[3]*Department of Mechanical and Aerospace Engineering, University of California, San Diego, California 92093-0411, USA*

(Received 19 May 2009; accepted 4 September 2009; published online 9 October 2009)

We demonstrate an experimental method to understand the mechanical response of carbon nanotube (CNT) ensembles to fluid flow through the measurement of the flexural rigidity *EI*, where *E* is the elastic modulus and *I* is the moment of inertia. A flexural rigidity (*EI*) of $\sim 7.5\times 10^{-16}$ N m^2 was determined for the samples examined, by monitoring the transmitted light intensity for the CNTs subject to flow induced deflections. The robustness of the measurements was revealed through the digital response of CNTs to fluid flow and their use in gas flow diagnostics. © *2009 American Institute of Physics*. [doi:10.1063/1.3238317]

I. INTRODUCTION

Carbon nanotubes (CNTs) have been found to have a remarkable combination of mechanical properties, incorporating high elastic moduli, *E* (for both single-walled[1] and multiwalled[2] CNTs), reversible bending and buckling[3] characteristics, and superplastic behavior at elevated temperatures.[4] However, in experimental measurements of the mechanical properties, while the applied loads and strains can be relatively easily configured and determined, it is not always practical to accurately measure the CNT cross-sectional area[5] for the calculation of stresses, or the moments of inertia (*I*). For example, simulations based on molecular dynamics yield a large discrepancy[6,7] in the *E* presumably due to this reason.[5] However, for the practical determination of the mechanical response of CNTs of varying lengths (*L*), subject to different forces (*P*), such as deflection under shear $(\Delta)=PL^3/3EI$ or critical buckling loads $(P_{cr})=\pi^2 EI/L^2$, the quantity of interest generally appears to be the *flexural rigidity*[8] *EI*. As the independent determination of *E* and *I* for CNTs can be difficult, we demonstrate a simple optical method to measure the combined *EI* value. Concomitantly, we seek to understand the mechanical behavior of nanotube ensembles, such as aligned CNT mats. Additional issues such as (a) varying tube-tube distances, (b) van der Waals interactions,[9] and (c) relative sliding of nanotubes[10] was also considered.

The flexural rigidity was determined through analyzing the CNT deflection, which was measured as a function of fluid flow induced drag forces, through the blockage of a laser beam and monitoring the transmitted intensity using a photodetector and CCD (Charge Coupled Device) camera based image processing. By fitting the experimental observations to deflections obtained using fluid flow simulations, the *EI* values were determined. We think that the principle of our methods can be extended for large scale applicability of CNTs in tactile and shear force sensing, e.g., in robotic applications, monitoring fluid flows,[11] security sensors, etc.

II. EXPERIMENTAL PROCEDURE

A. Synthesis of patterned vertically aligned CNT arrays

Patterned arrays of vertically aligned, multiwalled CNTs were synthesized from Fe catalyst films on quartz substrates, using thermal chemical vapor deposition (CVD). Prior to synthesis, the substrates were cleaned ultrasonically with acetone and isopropyl alcohol, and subsequently exposed to oxygen plasma (150 W for 30 s). A 5 nm thick Fe film was then deposited via electron beam deposition (at 10^{-6} Torr). The patterning of the Fe catalyst into arrays of blocks was achieved by shadow masking the substrate with a copper grid of specified pitch: 5×5 or 7×7 μm^2. The CVD process was initiated by heating the Fe catalyst coated quartz substrate to the growth temperature of ~ 900 °C in a reaction chamber, under an Ar and NH_3 mixture (1:1 ratio) flow (~ 500 SCCM) (SCCM denotes standard cubic centimeter per minute). When the furnace temperature was stabilized at 900 °C, benzene—the carbon source—was introduced into the chamber at 0.1 SCCM. The length of nanotubes grown using this process was determined to be proportional to the time of benzene flow; the CNT growth rate was approximately 4 μm/min, and little evidence of catalyst poisoning was observed. The average lengths and diameters of the CNTs used in this study were in the ranges 30–60 μm and 40–50 nm, respectively. Subsequent to growth, the CVD furnace was cooled under argon flow to room temperature.

B. Flow arrangement and optical measurements

For monitoring the response of the CNTs to fluid flow, the quartz substrate with the vertically aligned and patterned nanotubes was placed inside the experimental apparatus, illustrated in Fig. 1, consisting of a quartz tube (inner diameter of 6.2 mm) connected to a gas line. The CNTs were placed at

a)Electronic mail: pbandaru@ucsd.edu.

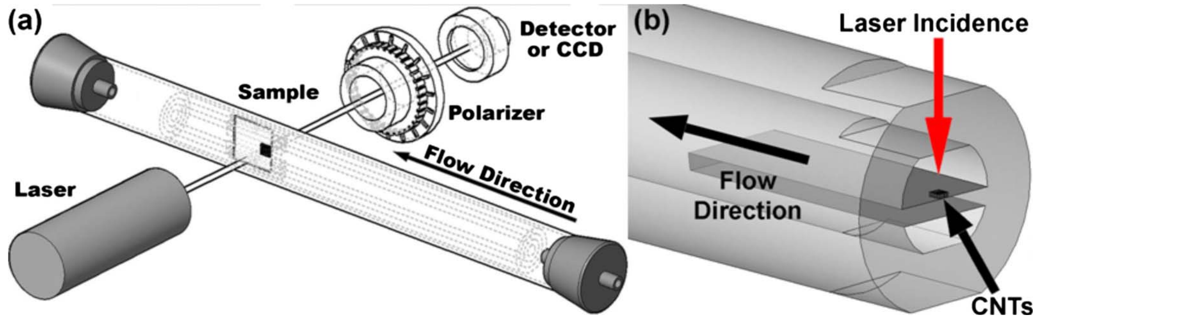

FIG. 1. (Color online) Schematic of the experimental setup for the observation of CNT deflections, due to fluid flow, by (i) monitoring the transmitted laser intensity variations and by (ii) CCD imaging. The insets illustrate the orientation of the CNT mats with respect to incident laser illumination.

the center of the tube and situated at the very front edge of the substrate and a polarized He–Ne laser (633 nm), focused to $\sim 30\ \mu$m spot size, was aligned parallel to the CNT axis and perpendicular to the substrate, as shown in Fig. 1. The samples were held in place by plastic inserts to prevent sample vibration, and were then exposed to fluid (air) at various pressures from which the velocities were calibrated using the flow chamber cross-sectional area and volumetric flow rates measured by a flow meter. A photodetector was used to monitor the transmitted intensity, which was then related to the CNT deflection at different fluid velocities. Independently, optical imaging of the CNT deflections was performed by a CCD camera (Sony N50, XC-75) aligned normal to the substrate. Scattering and refraction effects from the circular quartz tube surface were avoided by placing a flat quartz plate directly above the sample, and yielded reproducible and sensitive photodetector measurements and high resolution ($\sim 0.25\ \mu$m) CCD images.

On exposure to fluids, the deflection of the CNTs can be modeled by treating an individual tube, theoretically, as a fixed end cantilever system. Figure 2(a) illustrates the process by considering the *in situ* shearing of CNT arrays in a scanning electron microscope (SEM). The outline in the two figures on the right depicts the close correspondence between the theory and experimentally observed shear. As the CNT deflection reduces the incident laser intensity due to scattering and absorption, the transmitted laser intensity can be calibrated and correlated with the coverage of the CNTs on the substrate. For example, it was calculated that two CNT patterned arrangements, viz., (i) $90\times 90\ \mu\text{m}^2$ with a $127\ \mu$m pitch, and (ii) $38\times 38\ \mu\text{m}^2$ with a $64\ \mu$m pitch, are expected to transmit 50% and 35% of the light, respectively and indeed this was seen experimentally; see Fig. 2(b). The amount of CNT deflection was then calculated based on the intensity calibrations vis-à-vis pattern coverage. When the CNT mat pattern was aligned with the leading edge of the substrate, we model the deflection to be parallel to both the direction of fluid flow and the pattern rows; see Fig. 2(c). In the absence of fluid flow, the transmitted intensity (I_0) is proportional to the area initially devoid of the CNT mats, i.e., $A_{\text{total}}-L^2$. However, under fluid flow, the nanotubes deflect a distance d, covering an extra area (i.e., Ld) corresponding to a transmitted light intensity (I), which is now proportional to $[A_{\text{total}}-L(L+d)]$. Consequently, the ratio of the intensities before and after deflection is

$$\frac{I}{I_0}=\frac{A_{\text{total}}-L^2-Ld}{A_{\text{total}}-L^2}. \tag{1}$$

Direct CCD imaging of the CNTs, exposed to different flow velocities, was also used for cross-calibrating the deflections inferred from transmitted laser intensity measurements. It was noted that vibration due to fluid flow could cause a variation of the transmitted intensity. At ~ 65 m/s, the upper velocity limit in our measurements, a displacement of $\sim \pm 0.5\ \mu$m was seen- less than 20% of the measured CNT

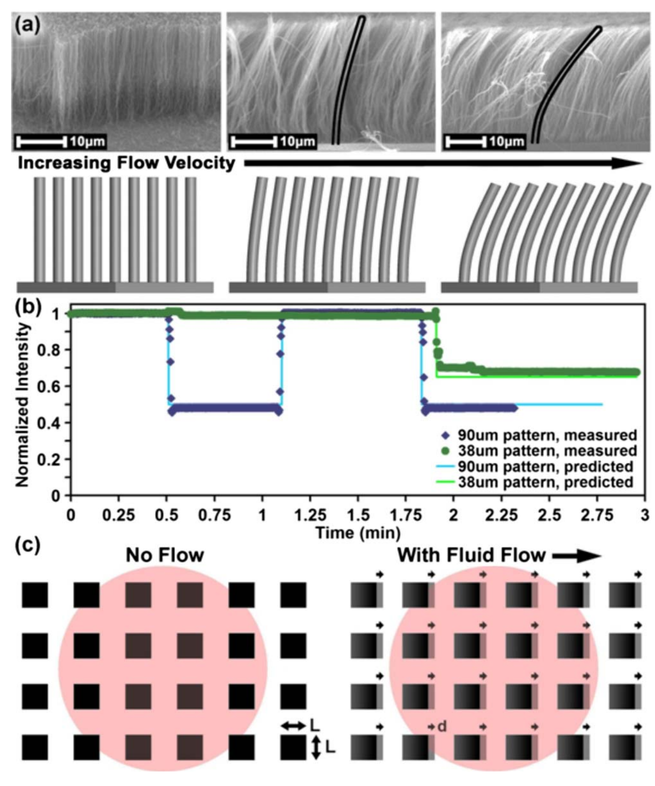

FIG. 2. (Color online) (a) The *in situ* shearing of CNT mats, as observed through SEM imaging, can be quite accurately modeled as through the deflection of a cantilever (as depicted by the outlines). (b) The calibration of the transmitted laser intensity was done by monitoring the transmission through CNT patterns arranged in a 90×90 and a $38\times 38\ \mu\text{m}^2$ pattern, respectively. An excellent agreement with predicted values, based on CNT coverage, was observed. (c) Modeling the effect of fluid flow on aligned CNT mats with a superposed circular laser spot. On exposure to fluid flow, the CNT displacement d is correlated with a measured variation in the laser transmission intensity and measured by a photodetector or monitored through CCD imaging.

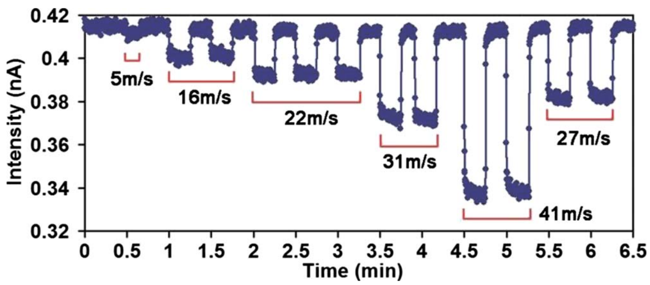

FIG. 3. (Color online) The variations in the transmitted laser intensity, through the CNT mats exposed to varying fluid velocities (i.e., 5, 16, 22, 31, 41, and 27 m/s), as a function of time. The robustness of the measurements is revealed in the *digital* response to various fluid velocities and return to a reference value when the flow is removed.

deflections. Such effects have been considered in recording the error of CNT deflection, and averaging over many measurements lowers error due to the area of the incident spot size.

III. RESULTS AND DISCUSSION

A. Modeling the response of the CNTs to fluid flow

An excellent correspondence was observed between the transmitted intensity and the air flow velocity (Fig. 3), and such a *digital* response was attributed to the mechanical robustness of the CNTs. Such correlation was observed very reliably for many measurements on the patterned CNT arrays, and the constant reference intensity in the absence of fluid flow attests to the flexibility of the CNT mats. To understand the effects of the drag forces induced by fluid flow (of velocity U and kinematic viscosity ν, $\sim 1.5 \times 10^{-5}\ \mathrm{m^2/s}$, and the density $\rho \sim 1.2\ \mathrm{kg/m^3}$ for air) on the CNTs, three characteristic length scales are of relevance, each associated with a Reynolds number Re as follows:

$$\mathrm{Re} = \frac{\rho U L}{\mu} = \frac{UL}{\nu}. \tag{2}$$

For L, the following are considered: (i) the diameter of the tube (~ 6.2 mm), for flow in the pipe; (ii) the distance from the leading edge to the sample, for flow over the substrate, modeled as a thin plate; and (iii) the diameter of the CNT, for flow through vertically oriented nanotubes. The Re for the air flow through the cylindrical pipe was in the range 8300–24 800 (for experimentally used velocities in the 20–60 m/s range), clearly[12] in the turbulent regime (Re$>$2300). Care was taken to avoid spurious fluid entrance effect by placing the CNT samples sufficiently inside the tube (~ 17 cm), beyond the entrance length L_e ($=4.4L\ \mathrm{Re}^{1/6}$) of ~ 14.7 cm calculated for $U \sim 60$ m/s. Beyond L_e, the fluid flow is considered fully developed, and the peak fluid velocity (U_{peak}), at the pipe center is related to the average velocity (U_{av}) through

$$U_{\mathrm{peak}} = \left[1 + \frac{0.722}{\log\left(\frac{\mathrm{Re}}{6.9}\right)}\right] U_{\mathrm{av}}. \tag{3}$$

As the CNT mats were grown close (<1 mm) to the leading edge of the quartz substrate, the Re in this region, $\sim 10^2$, is much smaller than that for turbulent flow ($\sim 10^6$), and the fluid flow over the substrate can be considered laminar. The boundary layer thickness δ at a distance x from the leading edge was computed through $\delta/x = 5/\mathrm{Re}^{1/2}$, to be in the range ~ 10–$100\ \mu$m. The velocity (U) profile considered as a function of the vertical height (y) is given by

$$U = U_{\mathrm{peak}}\left[2\frac{y}{\delta} - \left(\frac{y}{\delta}\right)^2\right] \quad \text{for } y > \delta, \tag{4a}$$

$$U = U_{\mathrm{peak}} \quad \text{for } y > \delta. \tag{4b}$$

It can then be inferred that for CNTs taller than the boundary layer height, the upper region of the tubes was exposed to the full centerline flow, i.e., $U = U_{\mathrm{peak}}$.

Due to the small CNT diameters (<50 nm), the Re for flow around the tubes was very small (~ 0.2 at $U = 60$ m/s). A modified Stokes–Oseen equation[13] was used to predict the drag coefficient C_D, assuming flow to be modeled as through a vertically aligned array of cylinders at low Re. The first bracketed term is related to the drag on a single cylinder, and the second bracketed term provides a correction for the volume fraction (ϕ) of the CNTs in a particular mat group:

$$C_D = \left[\frac{8\pi}{\mathrm{Re}_{\mathrm{S\text{-}O}} \ln\left(\frac{7.4}{\mathrm{Re}_{\mathrm{S\text{-}O}}}\right)}\right]\left[\frac{3 + 2\phi^{5/3}}{3 - 4.5\phi^{1/3} + 4.5\phi^{5/3} - 3\phi^2}\right]. \tag{5}$$

Equation (5) is based on conventional Navier–Stokes continuum mechanics,[13,14] where zero fluid velocity is assumed near the surface of the object, i.e., the no-slip boundary condition. At the size scales for flow through CNT mats, the no-slip assumption may not be accurate. However, the *form* of Eq. (5) seems to be in close correspondence with previous work on fluid flow past nanostructures. Good agreement with the macroscopic Stokes–Oseen equation was reported in nonequilibrium molecular dynamics[15] based simulations, which modeled water flow past single walled CNTs. While similar flow velocities were used in these simulations, the array density was lower and the C_D values fit a power law equation of the form $C_D = (9.0158/\mathrm{Re}^{1.0708})$. In modeling[16] the flow of liquid argon around both single- and double-walled CNTs, it was found that the drag was higher than predicted using continuum modeling and consequently, nonequilibrium molecular dynamics was used to fit $C_D = (12.354/\mathrm{Re}^{0.9887})$. In computational fluid dynamics based simulations[17] to study water flow around an array of nanotubes, using a *no-slip* assumption, $C_D = (86.7/\mathrm{Re})\phi^{0.287}$ and *with slip* $C_D = (39.9/\mathrm{Re})\phi^{0.175}$. The common theme in these studies seems to be the inverse dependence of the C_D to the Re.

To correct for the no-slip assumption in our model, a modification through the Knudsen number (Kn) was introduced.[18] The Kn is the ratio of the mean free path of molecules (λ) in the fluid to the characteristic length (L), and only for Kn$<$0.001 is the no-slip assumption valid. For our experiments, the Kn is around 0.5, assuming air at standard temperature and pressure, with $\lambda \sim 80$ nm, and an average CNT spacing, $L \sim 150$ nm. Consequently, slip at surfaces, which reduces the effective drag, must be considered. The incorporation of the slip condition then yields the following relation for C_D, where the first term was added to correct for surface slip:

$$C_D = \left[\frac{1+4\text{Kn}}{1+6\text{Kn}}\right]\left[\frac{8\pi}{\text{Re}_{\text{S-O}}\ln\left(\frac{7.4}{\text{Re}_{\text{S-O}}}\right)}\right] \times \left[\frac{3+2\phi^{5/3}}{3-4.5\phi^{1/3}+4.5\phi^{5/3}-3\phi^2}\right]. \quad (6)$$

Subsequent to the determination of C_D, the drag force per unit length F_D was derived by

$$F_D = \tfrac{1}{2}C_D U^2 A\rho \quad (7)$$

for a given CNT cross-sectional area A. This was then corrected for the implicit assumption of infinitely long cylinders, which implies uniform velocity over the entire CNT height, in Eqs. (5) and (6), i.e., the fluid velocity to which the CNTs are exposed is not constant along the entire height due to the boundary layer. To model and account for the varying U near the base of the CNTs, the CNT height h was divided into N segments, with a step size $\Delta y = h/N$. It was noted through our simulations that $N \geq 100$ was adequate for good representation. The U, C_D, and F_D were determined for each segment, at the corresponding height above the substrate, and A was taken to be the product of CNT diameter d and step height Δy. The horizontal displacement/deflection (x), as a function of position in the vertical direction (y), $x(y)$, was determined using a nanotube height dependent distributed drag force per unit length $w(y)$ through[8]

$$\frac{d^4x}{dy^4} = -\frac{w(y)}{EI}. \quad (8)$$

The differential equation was solved for $x(y)$, with the following assumptions and boundary conditions: (i) no shear at the CNT free ends ($d^3x/dy^3=0$, at $y=h$), (ii) no bending moments at the free end ($d^2x/dy^2=0$, at $y=h$), (iii) zero slope at the fixed end of the CNTs ($dx/dy=0$, at $y=0$), and (iv) zero deflection at the fixed end ($x=0$, at $y=0$). A procedure to allow for repeated numerical integration of the distributed load on the side of the tube was also developed. For each CNT segment of length Δy, the velocity profile *in the* boundary layer was calculated from Eq. (4a), while *above* the boundary layer, Eq. (3) was used. With the determined velocity distribution, the Re and the C_D were then calculated using Eqs. (2) and (6), respectively, for each Δy. The F_D on each segment (Δy) was determined by Eq. (7) to obtain the distributed loading along the entire CNT height, and this loading was integrated [Eq. (8)] using the trapezoid rule with the boundary conditions described above. Subsequently, the $x(y)$ was obtained for each segment along the nanotube height from Eq. (8). The main results obtained from these calculations are represented in Fig. 4. From Fig. 4(a), it was seen that the boundary layer thickness varies with fluid velocity and the placement of the CNT from the leading edge of the substrate. A smaller boundary layer thickness at larger velocities could imply that fluid velocity has a greater influence on deflection than the position of the CNT on the substrate. Consequently, a CNT (of height 50 μm) placed 100 μm from the leading edge would be deflected four times more ($\sim$5.2 μm) at 30 m/s compared to that at 10 m/s ($\sim$1.2 μm)—Fig. 4(b).

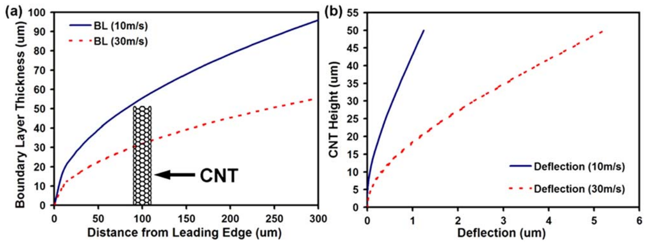

FIG. 4. (Color online) (a) Simulations of boundary layer thickness as a function of CNT distance from the leading edge of the substrate for fluid velocities of 10 and 30 m/s. (b) Simulations of nanotube deflections for velocities of 10 and 30 m/s, for CNTs 100 μm away from the leading edge.

B. Determination of the flexural rigidity *EI*

The flexural rigidity EI was approximated to be $\sim 10^{-15}$ N m^2, by calculating I through the parallel axis theorem ($I = \Sigma I_n + A_n d_n^2$), which is $\sim 5\times 10^{-24}$ m^4 for a (5×5 μm^2) CNT mat, using the experimentally determined value of E, $\sim$0.2 GPa. The E was obtained[19] through mechanical compression tests of CNT mats loaded normal to the tube axes—in the same direction as the drag, the details of which have been reported elsewhere.[19] This value of EI yielded an initial estimate. The EI was then determined through a best fit of the deflections calculated from our simulations, $x(y)$ to the experimentally measured deflections from nine samples. An iterative procedure, using MATLAB, was adopted with an initial EI estimate of 5×10^{-17} N m^2, which was subsequently varied in 5×10^{-17} N m^2 step sizes, with the total error (=difference between measured and simulated deflections) being obtained for each EI value. The value, which resulted in the lowest error, was used as an initial value for the next iteration. This process was continued until the convergence of the EI to a definitive value.

An EI of 7.9×10^{-16} N m^2 was determined [Fig. 5(a)] for deflections measured through transmitted laser intensity variations, while EI of 7.0×10^{-16} N m^2 was determined [Fig. 5(b)] for deflections measured through CCD based image processing. The very good agreement of the EI values obtained from two independent determinations of the deflections is remarkable. It is also noted that the obtained EI values correlated very well with previous studies of fluid flow past CNTs, and we have reported the correlation elsewhere.[11] The error in the EI determination mainly arises from the resolution of the CNT deflection yielding a maximum error of $\sim$10%, arising from parameters such as the CNT diameter (40–50 nm), length (30–60 μm), and spacing (100–200 nm) variation. Additionally, there could be an associated error due to the difficulty in determining the velocity profile close to the substrate. Consequently, the errors in EI's were estimated, assuming (i) pure turbulent and (ii) pure laminar velocity profiles, where it was seen that the difference of EI between cases (i) and (ii) was in the range 1%–10%. The higher error was obtained when the sample was

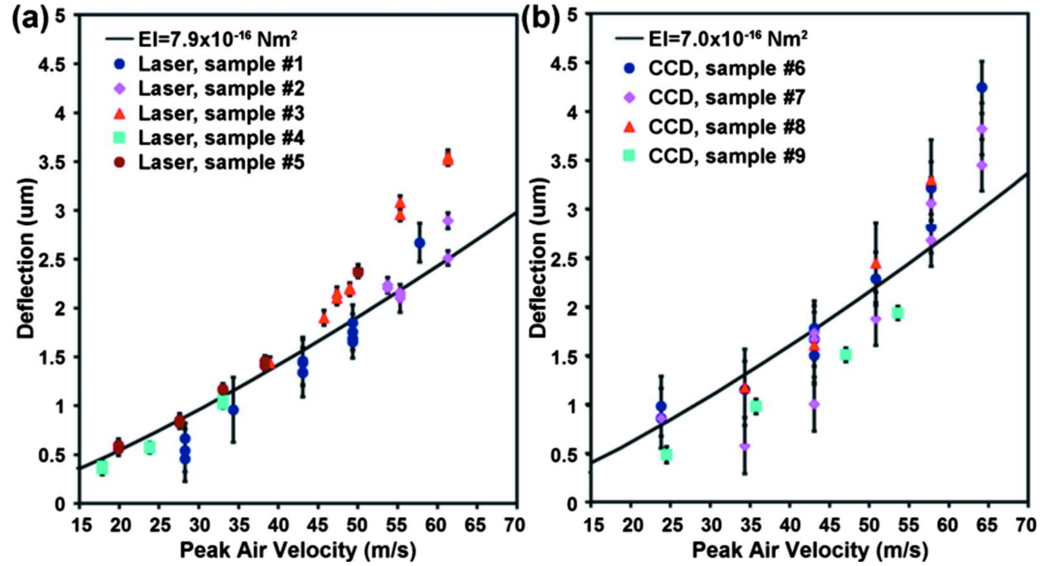

FIG. 5. (Color online) (a) The deflections of CNT mats, obtained through monitoring the transmitted laser intensity, as a function of air velocity, for five different samples. Numerical simulation was used to fit the *EI*, which is $\sim 7.9\times 10^{-16}$ N m^2. (b) The corresponding measurements of the deflections through CCD imaging yielded an *EI* $\sim 7.0\times 10^{-16}$ N m^2.

moved further away from the leading edge of the substrate, where the differences between turbulent and laminar flows become more pronounced. Sliding between adjacent CNTs due to van der Waals forces was also feasible, through which a nanotube ensemble/mat could exhibit a lower resistance to deflection than a rigid array. Consequently, the *EI* values would be expected to transition from one extreme—corresponding to a single, isolated CNT to another extreme: where with sufficiently large ensembles no additional resistance to bending is obtained due to CNT sliding.

C. CNT flow sensors

The remarkable robustness of the experimental results obtained on the deflection of CNTs and the understanding obtained through fluid flow modeling could be the basis for a new type of CNT based gas flow sensor. From Eq. (7), the drag force F_D exerted by the fluid on a CNT is a function of both the length scales (through C_D and A), along with the intrinsic properties (through the density ρ). It can then be inferred that the corresponding deflection $x(y)$ would vary linearly with ρ, at a given fluid velocity U. We assume that the ρ is proportional to the molecular weight (M) at a fixed temperature and pressure, and analyze the CNT deflections when exposed to different fluids. For example, deflections in argon flow compared to deflections in air would scale as $M_{\mathrm{Ar}}/M_{\mathrm{air}}$ ($\sim 40/29.2\approx 1.37$). This was indeed observed through the comparison of the transmitted light intensity as a function of (i) air, and (ii) argon flow velocities, and illustrated in Fig. 6. This result lends itself to the possible use of CNT ensembles for (i) accurately measuring the velocities of any fluid, with respect to a reference, e.g., air or argon, through simple density scaling, and more interestingly as a (ii) novel type of gas sensor.

IV. CONCLUSIONS

We have determined for the first time through experimental measurements, which were validated by detailed modeling, the flexural rigidity *EI* of CNT mats. The basis of measurement was the deflection of patterned arrays of CNTs subject to drag force, due to fluid flow, which was monitored optically. Our method, in addition to obtaining a numerical value for *EI*, ($\sim 7.5\times 10^{-16}$ N m^2 for the CNT samples under test), was useful for predicting the mechanical response of nanostructures. The robustness of the CNTs was revealed through their digital response to fluid flow and their use in gas flow diagnostics. Our method is capable of extension to finer resolution, e.g., limited by the precision of laser placement, and adaptable to the characterization of flow at the nanoscale including shear force sensors for boundary layer measurements and high sensitivity tactile force monitoring and gas sensing.

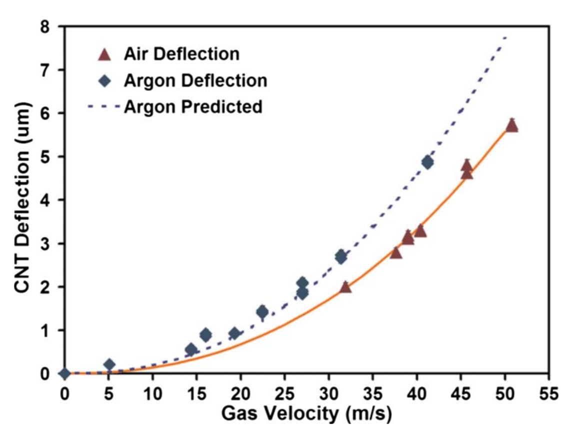

FIG. 6. (Color online) The CNT mat (5×5 μm^2 array) deflections were seen to be a function of both the nature of the fluid used (i.e., argon and air) and fluid velocity. We saw that by scaling the CNT deflections, subject to air, with the ratio of the argon density (ρ_{Ar}) and air density (ρ_{air}), the behavior of CNT samples in air can be very accurately predicted (as indicated by the argon predicted). The *EI* is $\sim 7.5\times 10^{-16}$ N m^2.

ACKNOWLEDGMENTS

Both C.P.D. and C.N. contributed equally to the project. We gratefully acknowledge support from the National Science Foundation (Grant Nos. ECS-05-08514 and DMI-0304019) and the Office of Naval Research (Award No. N00014-06-1-0234). P.R.B. acknowledges Dr. B. Fruhberger, and the staff at the Nano3 facility at CAL $(IT)^2$ in University of California, San Diego, CA.

[1]M.-F. Yu, B. S. Files, S. Arepalli, and R. S. Ruoff, Phys. Rev. Lett. **84**, 5552 (2000).
[2]M. M. J. Treacy, T. W. Ebbesen, and J. M. Gibson, Nature (London) **381**, 678 (1996).
[3]M. R. Falvo, G. J. Clary, R. M. Taylor, II, V. Chi, F. P. Brooks, Jr., S. Washburn, and R. Superfine, Nature (London) **389**, 582 (1997).
[4]J. Y. Huang, S. Chen, Z. Q. Wang, K. Kempa, Y. M. Wang, S. H. Jo, G. Chen, M. S. Dresselhaus, and Z. F. Ren, Nature (London) **439**, 281 (2006).
[5]Y. Huang, J. Wu, and K. C. Hwang, Phys. Rev. B **74**, 245413 (2006).
[6]J. P. Lu, Phys. Rev. Lett. **79**, 1297 (1997).
[7]B. I. Yakobson, C. J. Brabec, and J. Bernholc, Phys. Rev. Lett. **76**, 2511 (1996).
[8]F. P. Beer, J. E. R. Johnson, and J. T. DeWolf, *Mechanics of Materials*, 4th ed. (McGraw-Hill, Boston, MA, 2006).
[9]G.-W. Wang, Y. Zhang, Y.-P. Zhao, and G.-T. Yang, J. Micromech. Microeng. **14**, 1119 (2004).
[10]M. R. Falvo, R. M. Taylor, II, A. Helser, V. Chi, F. P. Brooks, Jr., S. Washburn, and R. Superfine, Nature (London) **397**, 236 (1999).
[11]C. Ni, C. P. Deck, K. S. Vecchio, and P. R. Bandaru, Appl. Phys. Lett. **92**, 173106 (2008).
[12]R. W. Fox and A. T. McDonald, *Introduction to Fluid Mechanics* (Wiley, New York, 1998).
[13]G. K. Batchelor, *An Introduction to Fluid Dynamics* (Cambridge University Press, Cambridge, 1967).
[14]J. H. Walther, R. L. Jaffe, T. Werder, T. Halicioglu, and P. Koumoutsakos, *On The Boundary Condition for Water at a Hydrophobic, Dense Surface*, Proceedings of the Summer Program, Vol. 317 (Center for Turbulence Research, Stanford University/NASA Ames, 2002).
[15]J. H. Walther, T. Werder, R. L. Jaffe, and P. Koumoutsakos, Phys. Rev. E **69**, 062201 (2004).
[16]W. Tang and S. G. Advani, J. Chem. Phys. **125**, 174706 (2006).
[17]A. Ford and D. V. Papavassiliou, Ind. Eng. Chem. Res. **45**, 1797 (2006).
[18]R. W. Barber and D. R. Emerson, "Numerical simulation of low Reynolds number slip flow past a confined microsphere," Daresbury, Lab. Technical Reports, DL-TR-2001–001, 2001.
[19]C. Deck, J. Flowers, G. S. McKee, and K. Vecchio, J. Appl. Phys. **101**, 023512 (2007).